Distribution of Landscape Types in the Global Historical Climatology Network

Laure M. Montandon*

Department of Geological Sciences, University of Colorado, Boulder, Colorado

Souleymane Fall

Department of Earth and Atmospheric Sciences, Purdue University, West Lafayette, Indiana

Roger A. Pielke Sr.

CIRES, University of Colorado, Boulder, Colorado

Dev Niyogi

Department of Earth and Atmospheric Sciences, and Department of Agronomy, and Indiana State Climate Office, Purdue University, West Lafayette, Indiana

Received 14 July 2010; accepted 13 August 2010

ABSTRACT: The Global Historical Climate Network version 2 (GHCNv.2) surface temperature dataset is widely used for reconstructions such as the global average surface temperature (GAST) anomaly. Because land use and land cover (LULC) affect temperatures, it is important to examine the spatial distribution and the LULC representation of GHCNv.2 stations. Here, nightlight imagery, two LULC datasets, and a population and cropland historical reconstruction are used to estimate the present and historical worldwide occurrence of LULC

* Corresponding author address: Laure M. Montandon, Department of Geological Sciences, University of Colorado, 2200 Colorado Ave., Boulder, CO 80309.
E-mail address: laure.montandon@colorado.edu

DOI: 10.1175/2010EI371.1

types and the number of GHCNv.2 stations within each. Results show that the GHCNv.2 station locations are biased toward urban and cropland (>50% stations versus 18.4% of the world's land) and past century reclaimed cropland areas (35% stations versus 3.4% land). However, widely occurring LULC such as open shrubland, bare, snow/ice, and evergreen broadleaf forests are underrepresented (14% stations versus 48.1% land), as well as nonurban areas that have remained uncultivated in the past century (14.2% stations versus 43.2% land). Results from the temperature trends over the different landscapes confirm that the temperature trends are different for different LULC and that the GHCNv.2 stations network might be missing on long-term larger positive trends. This opens the possibility that the temperature increases of Earth's land surface in the last century would be higher than what the GHCNv.2-based GAST analyses report.

KEYWORDS: Surface temperatures; Land cover; GHCN; Temperature trends

1. Introduction

The most recent Intergovernmental Panel on Climate Change (IPCC) report (Solomon et al. 2007) identifies greenhouse gases as the major climate forcing agent responsible for the increase in temperatures. Changes in land use/land cover (LULC) and ground albedo, however, also alter the energy balance of the climate (National Research Council 2005) and are now being considered with interest (De Noblet-Ducoudre and Pitman 2007; Pitman et al. 2009). To date, the scientific level of understanding of the role of LULC change (and subsequent changes in albedo and surface heat capacity) on climate forcing is low relative to that of greenhouse gases (Solomon et al. 2007). Many researchers, however, suggest that LULC changes can cause large local and regional temperature changes (Pielke and Avissar 1990; Shukla et al. 1990; Kalnay and Cai 2003; Kabat et al. 2004; Lim et al. 2005; Feddema et al. 2005; Pielke 2005; Chen et al. 2006; Hale et al. 2006; Hale et al. 2008; Cotton and Pielke 2007; Wichansky et al. 2008; Pielke and Niyogi 2010; Mahmood et al. 2010). This effect on temperature can be the result of changes in surface roughness, vegetation amount and type, and the alteration of surface heat and moisture fluxes. LULC differ over the world and have been unequally modified so that their distribution and the extent to which they have been anthropogenically altered vary.

Surface temperatures have been recorded at many locations around Earth for many decades. The Global Historical Climate Network (GHCN; Peterson and Vose 1997) regroups these recordings in one database that is the basis for most past temperatures reconstructions, including the well-known global average surface temperature (GAST) anomaly analysis (Hansen et al. 1999; Hansen et al. 2001; Jones and Moberg 2003; Smith and Reynolds 2005). The spatial distribution of these stations is heterogeneous (Figure 1), with some areas of the world being overrepresented (e.g., Europe and United States) and other areas being underrepresented (e.g., Russia, Africa, South America, and the polar regions). To correct for this bias, in addition to other known biases such as time of observations and instrument changes (e.g., see Pielke et al. 2000; Pielke et al. 2002; Pielke et al. 2007a; Pielke et al. 2007b), the GHCN temperatures are often averaged over smaller grid cells before being globally averaged to create a global world anomaly. The result is a more homogeneous appearing temperature record geographically.

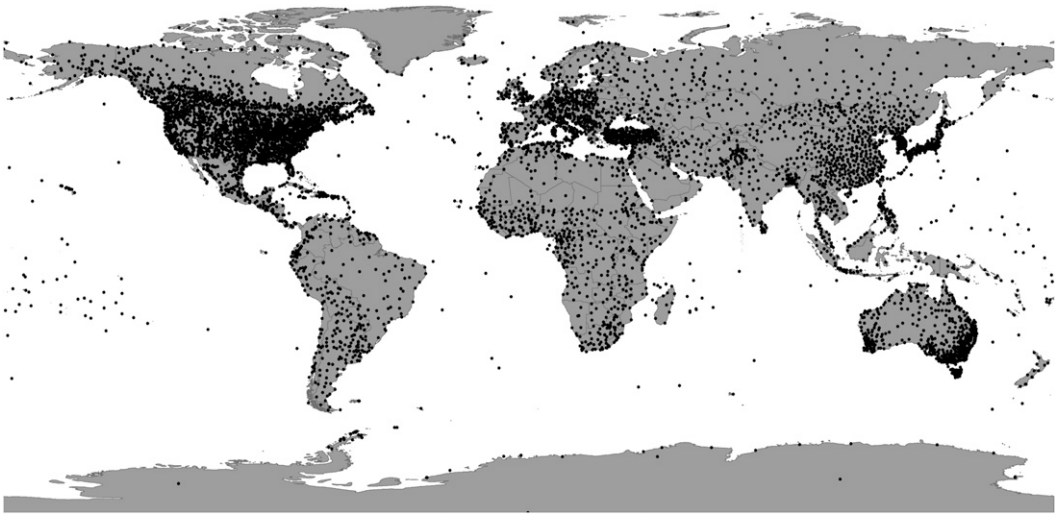

Figure 1. Spatial distribution of GHCNv.2 stations.

However, it is unclear if the station locations adequately represent each type of land cover found on Earth as well as LULC changes during the past several decades. This is an important assessment because of the recognized impact of land-cover transformations such as urbanization, deforestation, agricultural intensification, and practices such as irrigation on climate and therefore local temperatures (Foley et al. 2005; Roy et al. 2007; Turner et al. 2007; Fall et al. 2010a). There are also issues with the quality of the temperature data because of the local exposure of the surface temperature observing sites (i.e., Davey and Pielke 2005; Pielke et al. 2007a; Pielke et al. 2007b; Menne et al. 2010; Fall et al. 2010b, manuscript submitted to *J. Geophys. Res.*), but we do not consider this subject in this paper.

The goal of this paper is to assess the representation of the current GHCN monthly temperature dataset [version 2 (GHCNv.2)] used to compute the GAST anomaly in terms of its representation of global LULC and their changes since the 1700s. The assessment is guided from the results of many recent studies that suggest the LULC can impact the surface temperature trends (see Pielke et al. 2007a; Mahmood et al. 2010 for a recent review). Thus, the underlying principle is that any land-cover bias that exists in the GHCNv.2 dataset could introduce a positive (warming) or negative (cooling) bias in the GAST anomaly. This paper seeks to answer two major questions: (i) In what types of ecosystems and land cover are the GHCNv.2 stations located today? (ii) What are the historical population and cropland area changes at each GHCN v.2 station?

Unlike temperatures, land-cover change is a quantity that has not been measured continuously. Records of land-cover changes can rely only on historical records; inference of past human migrations; and, for the most recent years, satellite observations. Historical records and past population reconstructions can be subjective, and satellite observations, although useful, can have limited spatial resolution or temporal coverage. Further, the GHCN stations themselves show significant changes both in terms of the number of stations as well as changes in the station

history (Pielke et al. 2007a). Such limitations are inherent in a global monitoring network in wake of the regional development and also because the siting and distribution are often beyond the control of a single organization. In view of these inherent limitations, our results provide the first attempt at spatially assessing the distribution of the GHCNv.2 dataset in term of global land-cover representation.

2. Methods

2.1. Datasets description

2.1.1. Temperature stations

The GHCNv.2 temperature dataset regroups measurements from 7280 stations from around the world, all with at least 10 years of data. It also includes a subset of 5206 stations that is homogeneity adjusted so that discontinuities in the temperature record are corrected for biases due to changes in the instrumentation, time of observation bias, station moves, urban effects, and hand-checked exclusion of outliers from the original records (Peterson and Vose 1997; Peterson 2006; Pielke et al. 2007b). This second dataset is referred to here as the adjusted dataset. Each station of this dataset has at least 20 years of continuous data. The GHCNv.2 temperature dataset has been used by different research institutes to compute the GAST anomaly of the past century. The works of the following groups are the most commonly cited:

The Climatic Research Unit (CRU) at the University of East Anglia (Jones and Moberg 2003);
The National Climatic Data Center (NCDC) at the National Oceanic and Atmospheric Administration (Smith and Reynolds 2005); and
The Goddard Institute for Space Studies (GISS) at the National Aeronautics and Space Administration (Hansen et al. 1999; Hansen et al. 2001).

We obtained a list of stations that were used in the GAST analysis for all three datasets (CRU, NCDC, and GISS). NCDC uses data from all stations in the original adjusted GHCNv.2 dataset. GISS uses the unadjusted data from the GHCNv.2 dataset, separating the U.S. stations into a distinct subdataset [U. S. Historical Climatology Network (USHCN)] and carrying their own adjustment independently on both. The CRU dataset merges some of the GHCNv.2 data with their own temperature dataset to make it more comprehensive (Jones 1994), resulting in many stations that overlap between their final dataset and the GHCNv.2. The main steps in the stations selection of each dataset are summarized in Table 1.

The first step of our data preparation was to determine which stations in the three datasets are GHCNv.2 stations and determine the number of spatial duplicates (stations with same geographical coordinates). For each dataset, we created two subsets of stations. The first subset includes all stations (GHCN and non-GHCN) after removal of spatial duplicates, and it is used to compare station locations with historical LULC and population. The second subset includes only GHCNv.2 stations. Table 2 indicates the number of stations in each subset.

Typically, each temperature database would contain station numbers, names, and coordinates that could be matched to GHCNv.2 values. However, in the case of the

Table 1. Summary of land surface temperature datasets and stations selection methodology used by three research institutes computing GAST.

Research institute	Land surface temperature datasets used	Main steps of the analysis	Data exclusion criteria	No. of stations
CRU (Jones and Moberg 2003)	Joint Hadley Centre/University of East Anglia Climatic Research Unit temperature dataset (HadCRUT) currently on its third version, HadCRUT3 (Brohan et al. 2006), which merges data from many sources	Combination of multiple records at each station; data spatial homogenization over 5° × 5° grid; reference period: 1961–90	Stations more than 5 standard deviations from the long-term monthly mean; duplicates with shortest record	4138 stations (GHCNv.2 and other; available online at http://www.cru.uea.ac.uk/cru/data/landstations/)
NCDC (Smith and Reynolds 2005)	Adjusted GHCNv.2	Data spatial homogenization over 5° × 5° grid; reference period: 1961–90	Not specified	All GHCNv.2 adjusted stations
GISS (Hansen et al. 1999; Hansen et al. 2001)	Unadjusted GHCNv.2., including data from its U.S. subset (USHCN) through 2005; Scientific Committee on Antarctic Research (SCAR) data for the Antarctic	Combination of multiple records at each station–using the reference station method (Peterson et al. 1998); urban adjustment: nonrural stations are adjusted so that their long-term trends of annual mean are as close as possible to that of the mean of the neighboring rural stations; reference period: 1951–80	Less than 20 yr of combined record at the station; urban stations that could not be adjusted to neighboring rural values; stations more than 5 standard deviations from the long-term monthly mean	6257 GHCNv.2 stations (available online at http://data.giss.nasa.gov/gistemp/station_data/)

Table 2. Number of stations in each database and its two subsets.

	No. of stations in database	Size of first data subset (no spatial duplicates)	Size of second data subset (GHCNv.2 stations only)
CRU	4138, including 282 non-GHCNv.2 stations 100 spatial duplicates	4038	3756
NCDC	5206, including 435 spatial duplicates	4771	4771
GISS	6257, including 7 non-GHCNv.2 stations 21 spatial duplicates	6236	6229

CRU dataset, the stations numbers have sometimes been modified and geographical coordinates updated by CRU. It was therefore difficult to retrieve the specific list of matching GHCNv.2 stations. For this data subset, we selected all GHCNv.2 stations that were either matching the CRU station coordinates, had a similar station number, or had coordinates very close to the one provided by CRU (coordinate update is inferred). Therefore, the resulting CRU data subset is only an approximation of the GHCNv.2 stations used in the CRU analysis.

2.1.2. DMSP nighttime light imagery

To classify the present-day urban setting at each station, we used the thresholding method introduced by Imhoff et al. (Imhoff et al. 1997) that uses nighttime light imagery from the Defense Meteorological Satellite Program (DMSP; Elvidge et al. 1999) as a proxy for urban extent. The GHCNv.2 dataset includes information on population, but most of the data are based on the 1993 United Nations Demographic Yearbook (Peterson and Vose 1997) and therefore are no longer representative of present-day urban areas, particularly in regions that are undergoing a rapid pace of population growth and land transformation.

We used a recent nighttime light imagery: a 2003 cloud-free composite derived from all scenes available for this year from the DMSP Operational Linescan System (OLS) *F-15*, a low-light imaging capacity sensor originally developed to measure moonlight reflection off clouds. The product spatial footprint is 30 arc sec (2.7 km) and covers all world areas between −65° and 65° latitude. Pixel digital number (DN) values range from 1 to 63 and are proportional to the percent frequency at which light was detected over that pixel.

To relate night light intensity to urban extent, we used the thresholds established empirically by Imhoff et al. (Imhoff et al. 1997; Imhoff et al. 2000) to classify each station into three classes: unlit, dim, and bright corresponding to rural, peri-urban, and urban, respectively (Table 3). Imhoff et al. (Imhoff et al. 2000) correlated these thresholds to the following average population densities: 14 100 and 1064 inhabitants per square kilometer. These thresholds were also used as part of the temperature adjustment method GISS developed for their GAST analysis (Hansen et al. 2001).

2.1.3. GLCC v.2.0

The Global Land Cover Characterization (GLCC) database is a worldwide collection of land-cover classifications put together by the U.S. Geological Survey

Table 3. Nighttime imagery thresholds.

	Illumination (%)	Corresponding pixel DN	Avg POPD (inhabitants per km^2)
Rural	<8 unlit, noise	0–5	14
Peri-urban	8–88 dim	6–55	100
Urban	>88 bright	56–63	1064

(USGS), the University of Nebraska-Lincoln, and the Joint Research Centre of the European Commission. The dataset is primarily derived from 1-km Advanced Very High Resolution Radiometer (AVHRR) 10-day Normalized Difference Vegetation Index (NDVI) data. The imagery was acquired over a 12-month period between April 1992 and March 1993. This dataset was used to determine the area of the world occupied by specific land cover and ecosystems, as well as the ones found at temperature stations used in GAST computations.

We used two GLCC thematic maps: the International Geosphere Biosphere Programme (IGBP) land-cover classification (Belward 1996) and the Global Ecosystems (GE) classification (Olson 1994a; Olson 1994b). The IGBP divides the globe into 17 land-cover types. The GE classification divides the globe into 96 ecosystems based on land-cover mosaic, information on local floristic properties, and local climate. The complete list of these land covers and ecosystems can be found on the USGS GLCC Web site (available online at http://edc2.usgs.gov/glcc/).

2.1.4. HYDE 3 historical land-cover dataset

The History Database of the Global Environment (HYDE) dataset was used to estimate the portion of the world that has experienced urbanization and LULC changes since the 1700s, as well as the location of the temperature stations relative to these changes. This dataset is developed by the Netherlands Environmental Assessment Agency and comprises time series of population and land use in the form of gridded maps for the last 12 000 years (Klein Goldewijk 2001). The latest version of this dataset (version 3) has a 5 min × 5 min footprint and incorporates the information from recent databases on population density (POPD) and land cover at the subnational level. The methods and data sources used in developing the HYDE 3 dataset are described in Klein Goldewijk and van Drecht (Klein Goldewijk and van Drecht 2006).

For this analysis, we used the population density and cropland area between 1700 and 2000 (the most recent data available) at a 50-yr interval. Each yearly population gridded map shows the estimated population density expressed in inhabitants per square kilometer for each pixel. The cropland gridded maps show the area (in km^2) of crop for each pixel. Pixel area in this dataset varies with latitude, with the largest pixels being at the equator (85.9 km^2) and the smallest ones being at the poles (9.5 km^2). We divided the cropland area by the corresponding pixel size to be consistent when comparing the amount of crop in different areas of the world, creating maps of cropland density (CROPD) per pixel. Using both population and cropland datasets, we divided the data into classes described in Table 4.

Table 4. Population and cropland classes created from HYDE 3 data.

Class	Population (inhabitants per km^2)	Cropland (% pixel with crop)
1	0–10 (uninhabited)	0 (no crop)
2	10–1000 (small town)	0–25 (very low cropland)
3	1000–5000 (low density urban)	25–50 (low cropland)
4	5000–10 000 (urban)	50–75 (medium cropland)
5	≥10 000 (dense urban)	>75 (high cropland)

2.2. Analysis

2.2.1. Estimation of land-cover representation of the GHCNv.2 temperature stations

The first step of the analysis consisted in estimating the present-day relative occurrence of each land-cover class defined in section 2.1 both worldwide and within each temperature station's dataset. The analysis was carried out for the overall GHCNv.2 dataset and the CRU, GISS, and NCDC subsets of both GHCN and non-GHCN stations (note that the NCDC subset is equal to the adjusted GHCNv.2 dataset). Worldwide occurrence was established using the overall DMSP-OLS, GLCC, and HYDE datasets. Then the corresponding classes were assigned to each GHCNv.2 stations and the three subsets using their spatial coordinates.

2.2.2. Estimation of land-use/land-cover change to urban areas or croplands

The second step was to use the LULC historical data included in HYDE to estimate what percentage of the land has experienced urbanization and/or was transformed into cropland in the past century (1900–2000). We created two sets of change classes described in Tables 5 and 6. The HYDE population and cropland maps were divided into these classes, and the relative abundance of each class was computed. Each station from the GHCNv.2 dataset, as well as CRU, NCDC, and GISS subsets, was then assigned its corresponding change classes. The relative occurrence of each of these classes within each temperature stations datasets was then compared to their worldwide occurrence.

3. Representativeness of LULC by GHCNv.2 stations location

3.1. Present-day population and GHCNv.2 metadata

Using the 2003 nightlight imagery as a proxy for current population density, we see that only 5% of overall world land surface is lit. A large portion of the land (95%) is unlit and is associated to uninhabited or very low population density areas. Comparatively, the GHCNv.2 dataset and the three subsets are biased toward urban areas, as only 26.0%–31.1% of their stations are within rural (unlit) areas. There are a few issues associated to the use of nighttime light imagery to infer urban extent, with the most important one being the "blooming" effect: light tends to

Table 5. Description of POPD change classes for the period between 1900 and 2000.

POPD change class	Population change between 1900 and 2000	POPD in 1900 and 2000 (inhabitants per km^2)	2000 − 1900 POPD (inhabitants per km^2)
1	Pixel remained uninhabited	<10	
2	No POPD change		<±100
3	Population decrease		>−100
4	Small population increase		100–1000
5	Large population increase		>1000

extend beyond its associated populated area (Small et al. 2005). However, the results of the nightlight imagery urban classification are consistent with the one of the IGBP, GE, and HYDE 3 datasets (Table 7), suggesting an urban bias in the GHCNv.2 dataset of about 14% (although the HYDE 3 data suggest the bias might be slightly more).

The metadata provided with the GHCNv.2 contains information on the population at each of its stations. These data are based on population information that is now old (Peterson and Vose 1997) and do not reflect recent urban development. Hansen et al. (Hansen et al. 2001) used nightlight imagery to update the USHCN metadata. Here, we used the 2003 nightlight imagery classification to evaluate the quality of the GHCNv.2 metadata population classification. The GHCNv.2 stations are divided into three classes: 1) rural, where the population is less and equal to 10 000 people; 2) small town, where there are 10 000–50 000 inhabitants; and 3) urban, where there are more than 50 000 inhabitants. According to these metadata, more than half of the GHCNv.2 stations are located in rural areas (53.7%), whereas about 26.9% are in urban settings and 19.4% are in small towns (Table 7c). The three subsets are similarly divided, although the CRU subset has about 4% fewer stations in rural areas than the overall GHCNv.2 dataset.

With the 2003 nighttime light imagery, we find that only about 31.1% of the GHCNv.2 stations are located in truly unlit areas (Table 7a). The correspondence of this class to the GHCNv.2 metadata rural class is unclear due to the difference in

Table 6. Description of CROPD change classes for the period between 1900 and 2000.

Cropland change between 1900 and 2000	CROPD change class	CROPD in 2000–1900 (%)	2000–1900 CROPD (%)
Pixel remained uncultivated	1: Nonurban (rural or small town)	0	
	2: Nonurban (1900) to urban (2000)	0	
	3: Urban	0	
Cropland was reclaimed	4		−50 to −100
	5		0 to −50
Cropland increased	6		50 to 100
	7		0 to 50
Pixel kept very low crop amount	8	<25	
Density of crop remained unchanged	9	50 to 100 (high density)	0
	10	0 to 50 (low density)	0

Table 7. Population classification using (a) the 2003 nighttime light imagery; (b) the HYDE3 2000, the IGBP, and GE data; and (c) the GHCNv.2 population metadata.

(a) 2003 Nighttime light imagery classification

	Bright/urban (%)	Dim/peri-urban (%)	Unlit/rural (%)	No data
Subsets (No. of stations)	1064 inhabitants per km^2	100 inhabitants per km^2	10 inhabitants per km^2	
GHCNv.2 (7280)	15.0	51.7	31.1	2.2
CRU (4038)	18.1	53.0	26.0	2.9
NCDC (4771)	14.3	55.4	28.0	2.3
GISS (6236)	15.5	53.0	29.3	2.2
World land	0.3	4.7	95.0	

(b) Other datasets

	2000 HYDE 3 urban	2000 HYDE 3 small town	2000 HYDE 3 rural
	>1000 inhabitants per km^2	10–1000 inhabitants per km^2	<10 inhabitants per km^2
GHCNv.2 (7280)	18.1	56.4	25.5
World land	0.7	22.8	76.5
IGBP urban (%)			
GHCNv.2 (7280)	14.2		
World land	0.2		
GE urban (%)			
GHCNv.2 (7280)	13.7		
World land	0.2		

(c) GHCNv.2 stations population classification in metadata

	Urban (%)	Small town (%)	Rural (%)
Subsets (No. of stations)	>50 000 inhabitants	10 000–50 000 inhabitants	<10 000 inhabitants
GHCNv.2 (7280)	26.9	19.4	53.7
CRU (3756)	30.2	19.9	49.9
NCDC (4771)	26.3	19.0	54.7
GISS (6229)	27.6	19.4	53.0

their definitions: the unlit class is correlated with areas of 14 inhabitants per square kilometer (Imhoff et al. 2000), whereas the metadata urban class is linked to towns of $\leq$10 000 people with no mention of area. Under the assumption that the two are comparable, the current GHCNv.2 metadata overestimates by 22.6% the number of its stations located in rural settings, which is consistent with an increase in populated areas in the recent years.

3.2. Land-cover representation

Based on the IGBP dataset (16 classes, ignoring water bodies), the following land-cover types are the most common: open shrubland (14.1%), barren or sparsely vegetated (12.5%), snow and ice (12.4%), croplands (10.3%), and evergreen broadleaf forest (9.2%). Altogether they represent 58.5% of the total land area.

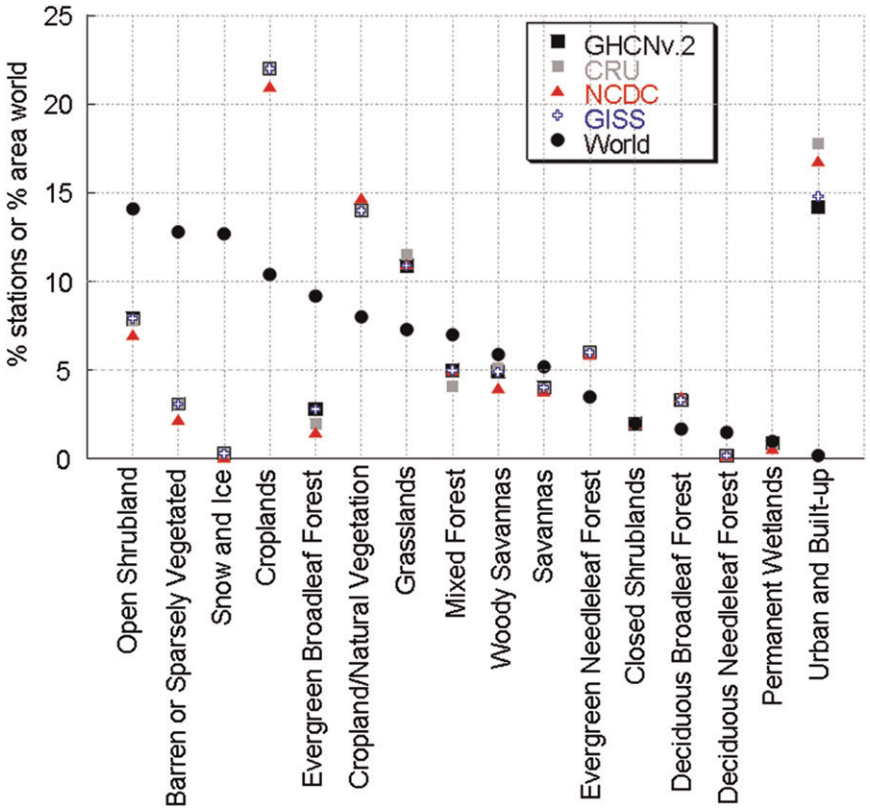

Figure 2. Percent land area covered by each IGBP land-cover class compared to the percent of temperature stations in each class.

Only 35.7% of all GHCNv.2 temperature stations are located within these land-cover types and about 32%–34% in the case of the CRU, NCDC, and GISS subsets. As a result, the main world land-cover types are not well represented by these stations.

The main land-cover types represented in the GHCNv.2 datasets and its three subsets (CRU, NCDC, and GISS) are croplands (18.9%–21.9%), urban and built up (14.2%–17.2%), cropland and natural vegetation mosaic (13.9%–14.7%), and grasslands (10.7%–11.5%). These areas make up about half the stations, whereas they only cover 18% of the world according to the IGBP data. This indicates that the temperature stations are biased toward areas affected by human activity (urban and cropland).

Figure 2 summarizes these results. The land-cover classes are classified from left to right according to their world abundance, from open shrublands (14.1%) to urban and built up (0.2%). The graph shows clearly how the relative abundance of each of these classes is different in the temperature stations dataset and subsets. Four out of the five main land-cover types are underrepresented in the temperature datasets. The exceptions are (i) croplands, which are overrepresented by about 10%, and (ii) urban and built up, which are overrepresented by 14.2% (GHCNv.2) to 17.2% (CRU).

Table 8. The 10 most common world ecosystems (seawater ignored) and percent of temperature stations within each. The gray shaded area highlights the 10 most abundant ecosystems in the temperature station dataset and subsets.

		Percentage of land area	Percentage of stations			
	GE class	World	GHCNv.2	CRU	NCDC	GISS
12	Glacier ice	12.1	0.5	0.5	0.3	0.5
8	Bare desert	10.5	2.4	2.6	1.9	2.4
33	Tropical rainforest	6.4	1.1	0.8	0.4	0.9
51	Semidesert shrubs	6.1	4.3	4.4	3.6	4.2
91	Woody savanna	5.1	3.9	4.1	3.4	3.8
43	Savanna (woods)	5.0	3.7	3.3	3.5	3.7
31	Crops and town	3.5	6.2	5.3	6.0	6.2
93	Grass crops	2.8	5.1	4.3	5.0	4.6
14	Inland water	2.4	3.4	3.3	3.5	3.3
9	Upland tundra	2.4	0.6	0.5	0.4	0.5
1	Urban	0.2	13.7	16.6	15.8	14.3
94	Crops, grass, shrubs	2.2	4.8	4.3	5.3	5.0
30	Cool crops and towns	0.8	3.7	3.5	4.0	3.6
41	Hot and mild grasses and shrubs	2.3	3.6	4.1	3.1	3.6

3.3. Ecosystems representation

Considering the GE dataset (95 classes, ignoring the seawater class, which represents 70.8% of the total area), the following ecosystems are the most abundant (Table 8): glacier ice (12.1%), bare desert (10.5%), tropical rain forest (6.4%), semidesert shrubs (6.1%), woody savanna (5.1%), and savanna (5.0%). Together they represent 45.2% of the land area. Only 15.8% of the GHCNv.2 stations are within these ecosystems and 13% of the NCDC subset stations (CRU and GISS stations distributions are comparable to the GHCNv.2 dataset).

The main ecosystems in the GHCNv.2 datasets and its three subsets are as follows (Table 8): urban (14.3%–16.6%), crops and town (5.3%–6.2%), grass crops (4.3%–5.1%), crops–grass–shrubs (4.3–5.3%), semidesert shrubs (3.6%–4.4%), and woody savanna (3.4%–4.1%). The IGBP classification results show that there is a clear bias toward urban and crop, which are both nonnatural ecosystems.

Figure 3 shows the 54 most common world land ecosystems classified in order of decreasing abundance from left to right. The percentage of stations in each class is also included. The graph shows the difference between the main world ecosystems and the location of temperature stations. It also outlines the urban and agricultural bias within these datasets. In the GE classification, only 0.2% of the land is classified as urban, whereas 13.7% of the GHCNv.2 stations are within urban boundaries (Table 8). These results are consistent with the data derived from both the IGBP urban land-cover data and the bright class of the nighttime light imagery. All of them suggest an urban bias of about 14% within the GHCNv.2 dataset, which is slightly enhanced (up to 3% more) by the selection of stations for each subset studied here.

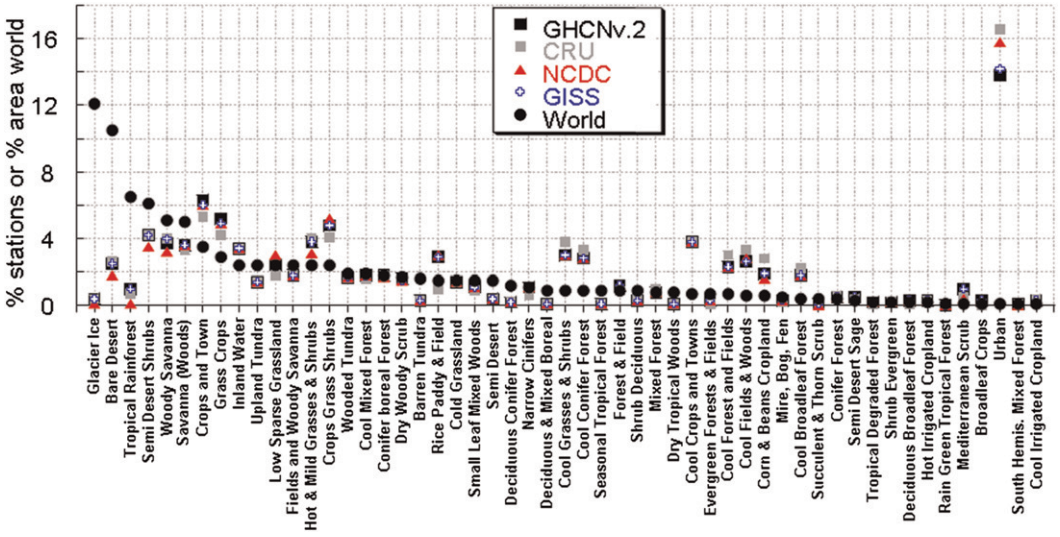

Figure 3. Percent land area covered by each GE ecosystem class compared to the percent of temperature stations in each class.

3.4. Urbanization

Figure 4a shows the change in world population density of the past 300 years as estimated from the HYDE dataset. In 1700, it is estimated that about 92% of the land was uninhabited, whereas the remainder had a low population density of

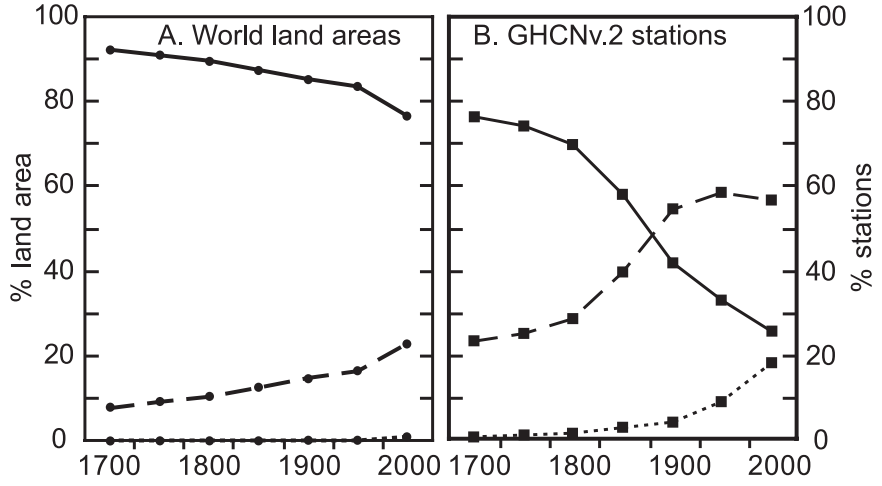

Figure 4. Percentage of (a) the world land areas and (b) the GHCNv.2 stations within each HYDE population class from 1700 to 2000: 1 (uninhabited; solid line), 2 (low POPD; dashed line), and 3–5 (urban; dotted line).

10–1000 inhabitants per square kilometer. The uninhabited areas of the world constantly decreased to 76.5% in 2000, whereas urban areas started to expand from the 1900s. World urbanization, however, still remains small in area, because in 2000 higher-density areas (>1000 inhabitants per square kilometer) are estimated to only occupy about 0.7% of the overall land surface. This is a little more than the percentage estimated from the bright class of the nighttime light imagery (0.3%) but of similar magnitude. Both approaches have inherent errors associated to the methodology used to compose the dataset, which can explain the slight percentage variability. For example, the population density distribution in the HYDE dataset is mostly based on countrywide population data. The population density was then extrapolated based on a reference map of population density under the assumption that high population areas remain in the same place over time (Klein Goldewijk 2001). This can potentially result in bias toward higher-density areas.

Figure 4b shows the corresponding percentage of GHCNv.2 stations for population classes (Table 4), with the three urban classes grouped into one. The location of the temperature stations shows a bias toward urban areas, whereas it underrepresents the uninhabited portions of the land. In 2000, 18.1% of the GHCNv.2 stations are identified as part of urban areas (17.5% more than the global percentage). Only 25.4% of these stations are within uninhabited areas. The subsets (CRU, GISS, and NCDC) exhibit similar distributions with respect to the overall GHCNv.2 dataset.

Figure 5 shows the population change classes defined in Table 5 and their relative occurrence between 1900 and 2000. During this period, about 75.6% of the land remained uninhabited. The remainder experienced urbanization or population increase (5.3%) or kept the same population density (19.1%). A negligible portion of the world experienced a decrease in population density. The location of the temperature stations relative to these changes is biased toward areas where population increased (by about 37%) or did not change (13.9%). This distribution depicts an underrepresentation of areas that remained uninhabited in the last century by 51.3%.

3.5. Cultivation

Figure 6a shows how the total area of cropland has expanded in the past 300 years. Areas with more than 50% cropland per square kilometer were occupying 0.3% of the land surface in 1700 and have expanded to 7% in 2000. Areas with no to very low crop [<25% $(km^2)^{-1}$] have consistently decreased from 98.7% in 1700 to 85.5% of the world surface in 2000.

Figure 6b shows the corresponding percentage of GHCNv.2 stations within each of the four cropland density classes. A quarter of the GHCNv.2 stations are located in areas that were densely cultivated (>75% cropland per square kilometer) between 1900 and 1950 when only 2% of the overall global land cover belonged to that class. As a result, areas that had none to a small amount of cropland (<25% crop per square kilometer), particularly in the past 150 years, are 34.9% underrepresented by the location of the temperature stations (see the dip of the solid black line on Figure 6b).

Figure 7 depicts the cropland change classes defined in Table 6 and their relative occurrence between 1900 and 2000. In the past century, 43.2% of the world

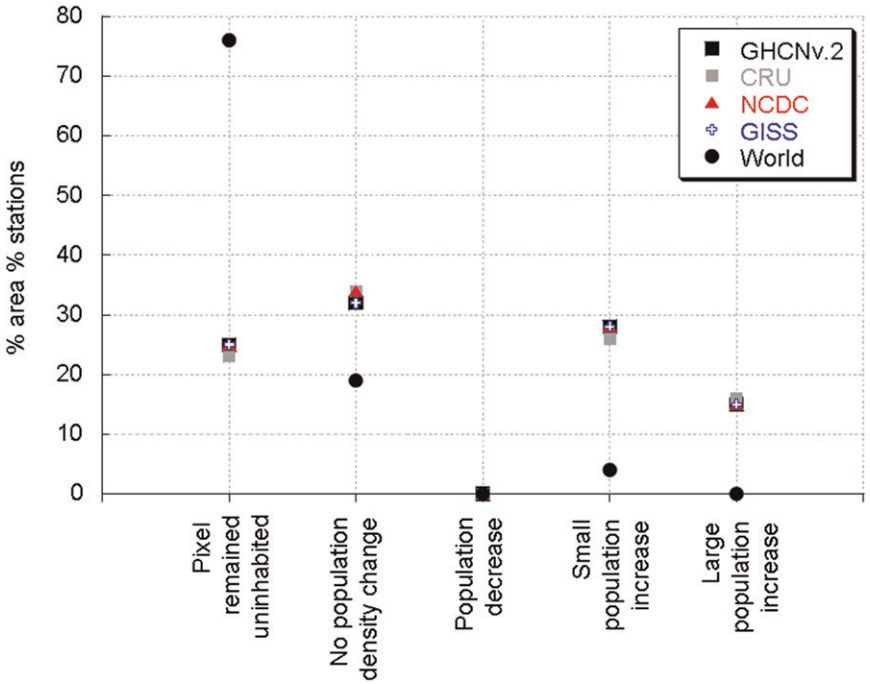

Figure 5. Percentage of the world land areas and temperature stations within each population change class for the period between 1900 and 2000 (see Table 5).

remained nonurban uncultivated land, suggesting that the natural environment was likely preserved in those areas (although this classification does not differentiate from, e.g., areas where deforestation has occurred). More than one-third of the land (36.5%) kept a very low density of crop (<25%), and 12.3% of the world experienced an increase in cropland areas. The spatial distribution of the temperature stations and subsets represent well the areas where cropland density has increased or remained unchanged. However, the distribution underrepresents areas that remained potentially natural (change class 1) by 29.3%. Finally, areas where cropland density has decreased are overrepresented by 33.6%. This decrease in crop area is, in general, associated with a local increase in population.

4. Discussion

The percentage of GHCNv.2 stations within urban areas is 13.7%–18.1%, depending on the classification used (2003 nightlight imagery, IGBP, GE, or HYDE 3). Comparatively, the percentage of the world land that is urbanized is 0.2%–0.3% (corresponding to the land portion that is bright on the nightlight imagery and the urban classes in the IGBP and GE datasets). This indicates that the locations of temperature stations are biased toward urban areas by 13.5%–17.9%, depending on the subset and classification method. The station distribution within the other land-cover classes shows that about one-third of the stations are located in

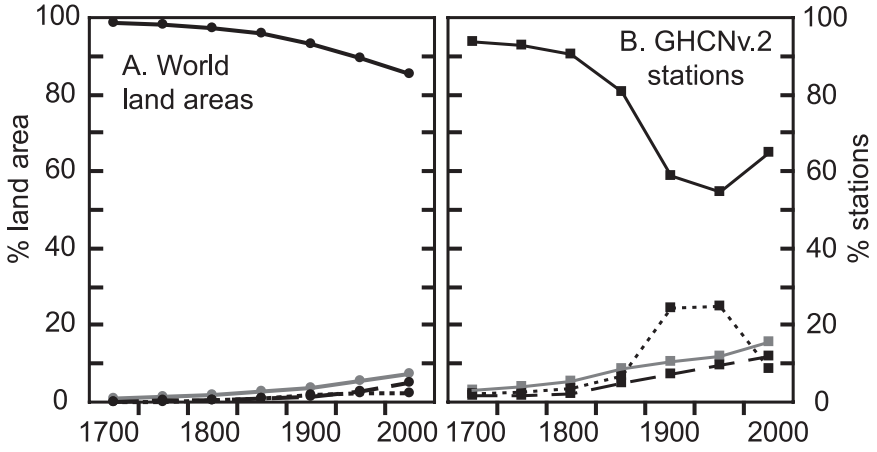

Figure 6. Percentage of (a) the world land areas and (b) the GHCNv.2 stations within each HYDE cropland class from 1700 to 2000: 1–2 (uncultivated or very low crop; solid black line), 3 (low crop; solid gray line), 4 (medium crop; dashed black line), and 5 (high crop; dotted black line).

cultivated land (cropland classes). Including stations in urban settings, they represent about 50% of the stations. Consequently, at least half of the GHCNv.2 temperature dataset was measured in areas where human-induced land-cover change is a major component in the station history. Also, the location of these

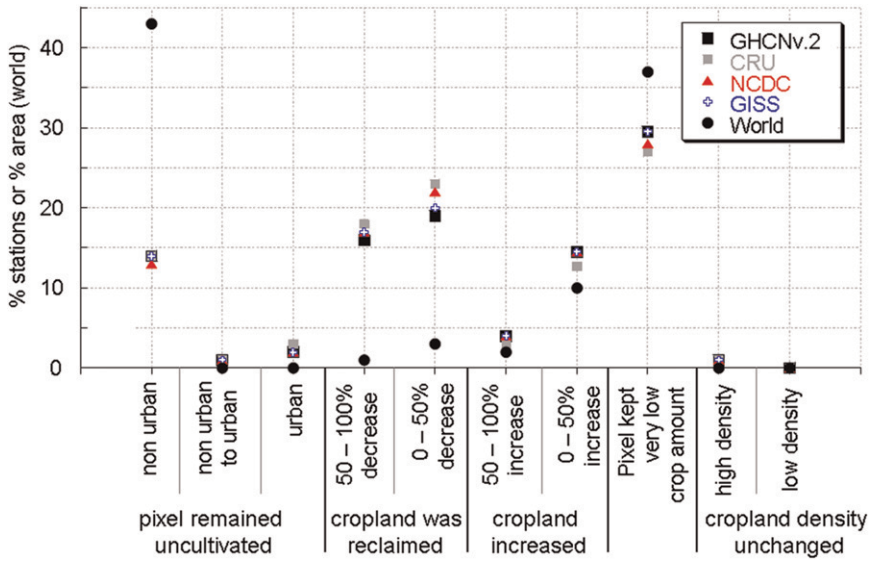

Figure 7. Percentage of the world land areas and temperature stations within each cropland change class for the period between 1900 and 2000 (see Table 6).

stations overrepresents the urban and in particular the cropland classes compared to their spatial extent worldwide (only 18.4% of the land worldwide).

On the other hand, widely spread land cover such as open shrubland, bare/sparsely vegetated, snow/ice, and evergreen broadleaf forests (48.1% of the land worldwide) are largely underrepresented in the GHCNv.2 dataset, with only 14% of the stations within these LULC types. The ecosystems classification yields similar results: glacier ice, bare desert, semidesert shrubs, and tropical forests, which occupy 35.1% of the world land area according to Olson classification (Olson 1994a; Olson 1994b), are represented only by 8.2% of the GHCNv.2 stations (and only 6.1% of the adjusted subset, NCDC). Note that the different subsets of stations studied here (CRU, GISS, and NCDC) have little impact on these classification results.

The 1900–2000 historical record of urbanization shows that, as expected, the locations of the GHCNv.2 and subsets stations are strongly biased toward regions where population has increased (by about 37%). This distribution results in underrepresentation of areas that remained uninhabited during the past century. In the total land areas, 75.6% of the areas were identified as having remained uninhabited, whereas only about 25% of the stations were within those areas.

With regard to the past century evolution of cultivated land, GHCNv.2 and the three stations subsets represent well areas that have either been and remained cultivated or the areas where the amount of cropland has increased. However, land areas where the amount of crop has decreased are overrepresented in those datasets by 31.6% (GHCNv.2 stations) to 36.2% (CRU stations subset). Finally, areas that were nonurban and remained uncultivated between 1900 and 2000 are underrepresented by about 29%, again suggesting that the temperature stations tend to be in areas where manmade LULC changes have occurred.

5. Potential implications of the LULC distribution on GAST

To provide a perspective on what the findings regarding LULC distribution could potentially mean, we conducted an initial assessment by computing the decadal anomaly trends for the different datasets. The trends reported here are the average of all trends from all stations within each LULC class. The decadal temperature trend at each station was computed by removing the temperature annual cycle to extract monthly-mean temperature anomalies. A linear trend analysis (least squares method) was performed on the anomalies using the overall temperature record available at each station. The record length varies significantly between stations (from 20 to 289 years), starting as early as 1702 (station 10384 in Berlin, Germany) and ending in 2008. The decadal temperature trends were then grouped according to the classes defined earlier and summary statistics were computed for each class, including the mean decadal temperature trend and its 95% confidence interval. A summary of the trends is presented in Figures 8a–g. The analysis was done with trends based on present-day population classification following 2003 nighttime light imagery (Figure 8a), as well as IGBP land cover (Figure 8b), Global Ecosystems (Figure 8c), HYDE population density in 2000, and past century changes (Figures 8d–g).

The results are generally comparable and only a subset from the IGBP land cover is discussed for brevity. The averaged decadal trend for 14 IGBP classes

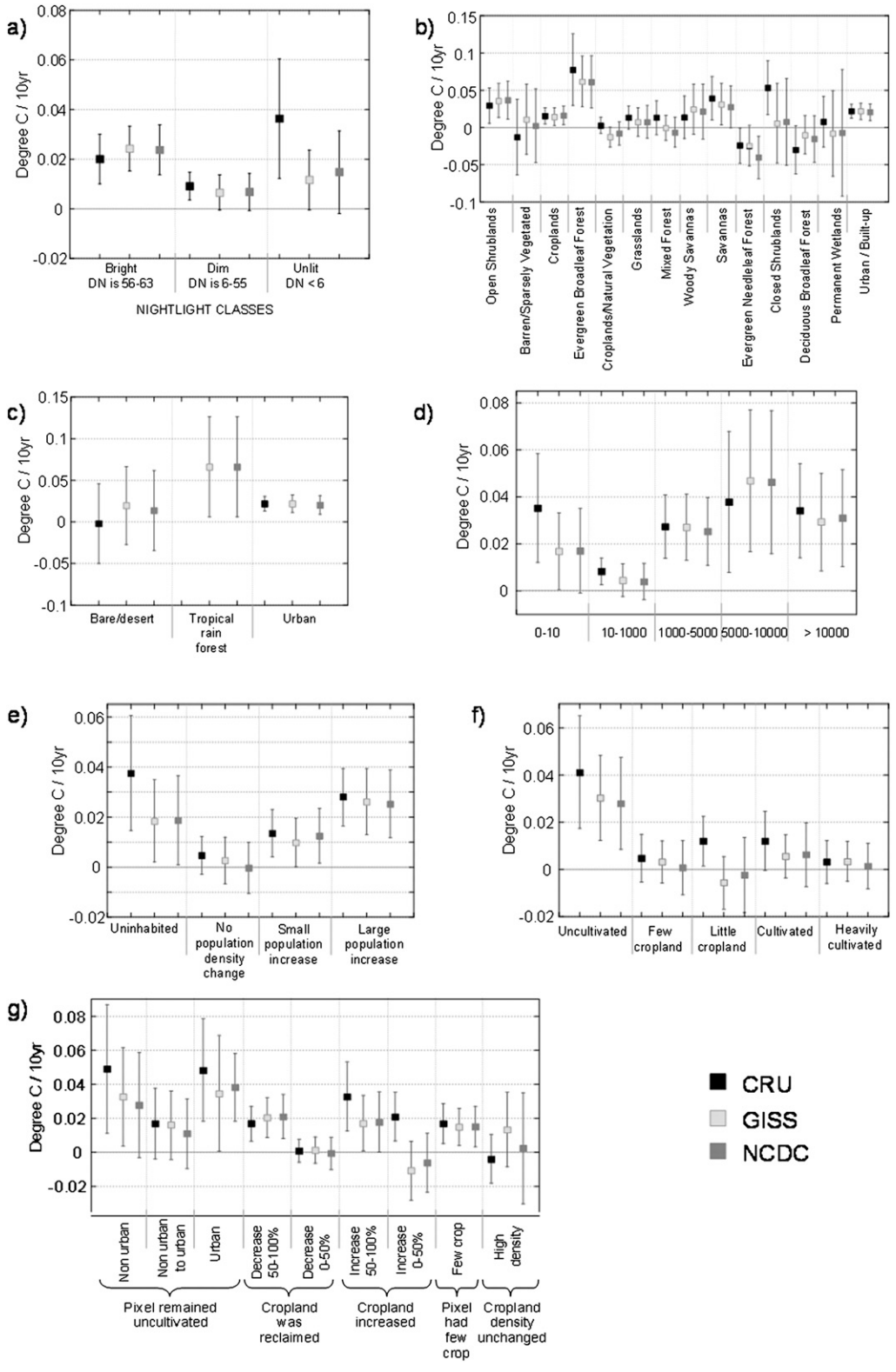
a)
Degree C / 10yr
0.08
0.06
0.04
0.02
0
-0.02
Bright DN is 56-63
Dim DN is 6-55
Unlit DN < 6
NIGHTLIGHT CLASSES
b)
Degree C / 10yr
0.15
0.1
0.05
0
-0.05
-0.1
Open Shrublands
Barren/Sparsely Vegetated
Croplands
Evergreen Broadleaf Forest
Croplands/Natural Vegetation
Grasslands
Mixed Forest
Woody Savannas
Savannas
Evergreen Needleleaf Forest
Closed Shrublands
Deciduous Broadleaf Forest
Permanent Wetlands
Urban / Built-up
c)
Degree C / 10yr
0.15
0.1
0.05
0
-0.05
-0.1
Bare/desert
Tropical rain forest
Urban
d)
Degree C / 10yr
0.08
0.06
0.04
0.02
0
0-10
10-1000
1000-5000
5000-10000
> 10000
e)
Degree C / 10yr
0.06
0.04
0.02
0
-0.02
Uninhabited
No population density change
Small population increase
Large population increase
f)
Degree C / 10yr
0.06
0.04
0.02
0
-0.02
Uncultivated
Few cropland
Little cropland
Cultivated
Heavily cultivated
g)
Degree C / 10yr
0.08
0.06
0.04
0.02
0
-0.02
Non urban
Non urban to urban
Urban
Decrease 50-100%
Decrease 0-50%
Increase 50-100%
Increase 0-50%
Few crop
High density
Pixel remained uncultivated
Cropland was reclaimed
Cropland increased
Pixel had few crop
Cropland density unchanged
CRU
GISS
NCDC

ordered from the most (left) to the least (right) abundant worldwide is shown in Figure 8b. Two classes that include less than 15 temperature stations are shown in Figure 8b: snow/ice (third most common IGBP class worldwide) and deciduous needleleaf forest. The long-term trend of the past 300 years reveals that four of the five most common land-cover types worldwide, which cover >58% of the land, show a positive temperature trend. The snow/ice class displays the largest average positive trend (0.32°–0.35°C decade^{-1}). Other significant long-term positive temperature trends in common LULC occur in evergreen broadleaf forests (0.061°–0.077°C decade^{-1}) and in open shrublands (0.029°–0.037°C decade^{-1}). Comparatively, most of the GHCNv.2 temperature stations are located in land-cover classes that have a relatively moderate positive temperature trend (e.g., urban and built-up areas: 0.021°–0.022°C decade^{-1}; cropland: 0.014°–0.016°C decade^{-1}). This indicates that, in its current distribution, the GHCNv.2 dataset may miss the largest long-term positive temperature trends. Savannas and woody savannas also experience long-term positive temperature trends (0.03°–0.04° and 0.01°–0.02°C decade^{-1}, respectively) but occupy a small portion of the world's land (2.4%). A few negative long-term temperature trends are found in evergreen needleleaf forests (−0.02° to −0.04°C decade^{-1}) and deciduous broadleaf forests (−0.01° to −0.03°C decade^{-1}), both classes that are weakly represented worldwide (4.8% of the world area), and in cropland/natural vegetation mosaic (−0.013° to 0.002°C decade^{-1}), which covers 7.9% of the world land. Trend analysis of other IGBP classes reveals mixed results: CRU decadal trends are sometimes of opposite sign to the GISS and NCDC trends (e.g., mixed forests, permanent wetlands, and bare). Differences in the magnitude of trends are also observed between the datasets in the case of the closed shrubland class; CRU mean trend is 0.053°C decade^{-1} versus 0.006° and 0.008°C decade^{-1} for GISS and NCDC, respectively. Such discrepancies may be partly explained by the large differences in station number: in general, GISS and NCDC have twice as many stations as our CRU subset, resulting in a better global distribution.

Decadal temperature anomaly trends of stations located in GE classes are shown in Figure 8c. Because of the large number of classes, the trends were computed only for a selected number of GE classes: glacier ice, bare desert, tropical rain forest (three most abundant classes worldwide), and urban. The largest positive temperature trends (0.32°–0.35°C decade^{-1}) are observed in the glacier ice class. Long-term trends of bare/desert ecosystems, the second-most abundant ecosystem worldwide, are weak: slight positive trends for GISS and NCDC (0.01°–0.02°C decade^{-1}) stations and slight negative trends for CRU (−0.002°C decade^{-1}). Tropical rain forests (third-most abundant ecosystem) exhibit a positive trend (0.07°–0.09°C decade^{-1}), which is similar to the long-term positive trend identified in the evergreen broadleaf

←

Figure 8. Mean decadal temperature anomaly trends for the groups of CRU, GISS, and NCDC stations with overall temperature record available at each station for (a) land classes derived from 2003 nighttime light imagery; (b) IGBP land-cover classes; (c) GE ecosystem classes; (d) HYDE POPD classes in 2000; (e) HYDE POPD change from 1900 to 2000; (f) HYDE crop density classes in 2000; and (g) HYDE crop density change from 1900 to 2000.

forest IGBP class (Figure 8b). The urban ecosystem represents only 0.2% of the GE ecosystems but is largely overrepresented in the GHCNv.2 dataset. All subsets agree in showing a slight long-term positive temperature trend (0.02°C decade^{-1}), consistent with the one observed in the IGBP urban class.

The mean long-term decadal temperature anomaly trends of stations grouped according to population density in 2000 (defined in Table 4) are shown in Figure 8d. All populated areas are characterized by long-term positive temperature trends. Stations located in urban areas (5000–10 000 inhabitants per square kilometer) exhibit the largest trends (0.04°–0.05°C decade^{-1}), followed by stations in dense urban areas and low-density urban areas (both 0.03°C decade^{-1}). Small towns (10–1000 inhabitants per square kilometer) experience very little temperature increases (0.004°–0.008°C decade^{-1}). The uninhabited stations also show average long-term positive temperature trends (0.02°–0.04°C decade^{-1}) similar to the one identified in the unlit class of the 2003 nighttime imagery.

Figure 8e displays the mean long-term decadal temperature anomaly trends of stations population change classes (as defined in Table 5 for 1900–2000). The ''population decrease'' class, with only four stations, is excluded from the analysis (this class is also insignificant worldwide, with less than 0.1% of the land). All subsets agree in showing positive temperature trends increasing with population density change (e.g., 0.03°C decade^{-1} in areas that experienced large density increase). Areas with no population density change show no significant trend (0.000°–0.005°C decade^{-1}). In areas that remained uninhabited, trends vary from 0.02° to 0.04°C decade^{-1}.

The long-term mean decadal temperature anomaly trends of stations grouped according to crop density classes in 2000 (Table 4) are displayed in Figure 8f. For all subsets, the largest positive trend occurs in stations located in uncultivated areas (0.03°–0.04°C decade^{-1}). Cultivated areas exhibit relatively little temperature changes (0.00°–0.01°C decade^{-1}), in agreement with the results found in the IGBP cropland class (0.01°–0.02°C decade^{-1}).

Figure 8g shows the long-term decadal temperature anomaly trends of stations grouped according to crop density changes over the past century (as defined in Table 6). Class 9 (density of crop remained unchanged; low density) is only represented by one station in all subsets and as a result has been removed from the analysis (it also represents a negligible portion of the land worldwide, as shown in Figure 7). For most of the change classes, a positive temperature trend is observed, with the largest ones (0.03°–0.05°C decade^{-1}) occurring in areas that remained uncultivated (nonurban and urban). In cultivated zones, changes in crop density seem to affect temperature trends: areas where the cropland density increased by more than 50% exhibit positive trends (0.02°–0.03°C decade^{-1}) as well as areas where cropland decreased by more than 50% (0.02°C decade^{-1}). Areas with small increase or decrease in cropland surface (0%–50%), however, show weakly positive or negative trends (e.g., −0.01°C decade^{-1} for GISS and NCDC).

6. Conclusions

Using over 5000 stations and different LULC datasets, a synthesis regarding the representation of the current GHCN monthly temperature dataset (GHCNv.2) was successfully conducted.

Our results confirm the findings from Hansen et al. (Hansen et al. 2001) that the GHCNv.2 metadata are outdated. According to the 2003 nighttime light imagery classification, the metadata overestimate the percentage of stations within rural (unlit) areas by 22.6%. Consequently, the stations classified as being within urban and small towns are underestimated in the GHCNv.2 metadata. The results of the nightlight classification are consistent with the ones from the IGPB, GE, and HYDE 3 datasets and confirm the robustness of nightlight imagery as a proxy for urban/rural areas.

Long-term temperature trends in cropland areas of the world show a slight positive trend (0.01°–0.02°C decade^{-1}), whereas urban classes exhibit slightly higher values (0.02°C decade^{-1} on average and increases up to 0.05°C decade^{-1} with population density). These results are in agreement with urban warming studies such as those reported in Oke (Oke 1987) and Oke and Hay (Oke and Hay 1998). These two classes, which are overrepresented in the GHCNv.2 dataset, have smaller long-term positive temperature trends compared to more abundant land-cover classes worldwide such as open shrublands (0.03°–0.04°C decade^{-1}) and evergreen broadleaf forests (0.06°–0.08°C decade^{-1}). This indicates that the GHCNv.2 may be missing larger regional long-term positive land temperature trends. As a result the long-term land surface temperature increases would be higher than indicated by the GHCN-based GAST analyses during the time period of this record.

The evolution of cultivated land over the past century shows that the GHCNv.2 and the three stations subsets represent well areas that have been and remained cultivated or where the amount of cropland has increased. However, land areas where the amount of crop has decreased are overrepresented by 31.6% (GHCNv.2 stations) to 36.2% (CRU stations subset). Finally, areas that were nonurban and remained uncultivated between 1900 and 2000 are underrepresented by about 29%; such a distribution suggests that the temperature stations tend to be in areas where manmade LULC changes have occurred. The largest positive temperature trends of all crop change classes (0.03°–0.05°C decade^{-1}) occur in the overrepresented ''areas remained uncultivated and nonurban'' class, whereas the underrepresented ''cropland was reclaimed'' class shows smaller trends (0.00°–0.02°C decade^{-1}). These results again suggest that GAST computations from GHCNv.2 data could have missed larger positive temperature trends over the period of record.

The scientific level of understanding on how LULC affect climate is low and the scientific community should focus on better understanding the related impacts, improving the global distribution of temperature stations network, and updating the descriptions of the LULC and other metadata for each station (including photographic documentation) to address this issue. The analysis presented in this paper should also be updated with more recent temperature datasets and land-use metadata. The trend analysis exercise was undertaken to gain a perspective on the potential impact of the land-cover distribution on the surface temperatures, and it should be repeated in a more formal manner with historical land-use change data, more detailed metadata, and up-to-date datasets in a follow-up study.

Acknowledgments. The authors want to thank Dallas Staley for her reading and suggesting final editorial edits to the paper. The study benefited from NSF CAREER (L. Zhou, A. Bumzai, E. DeWeaver). R. Pielke Sr. was also supported for his part in this study by the SAIC Consulting Agreement 653995 and F/DOE/The University of Alabama

in Huntsville's Utilization of Satellite Data for Climate Change Analysis (DE-FG02-04ER 63841) through the University of Alabama at Huntsville and by CIRES/ATOC at the University of Colorado, Boulder.

References

Belward, A. S., 1996: The IGBP-DIS global 1 km land cover data set (DISCover)—Proposal and implementation plans. IGBP-DIS Working Paper 13., 61 pp.

Brohan, P., J. J. Kennedy, I. Harris, S. F. B. Tett, and P. D. Jones, 2006: Uncertainty estimates in regional and global observed temperature changes: A new dataset from 1850. *J. Geophys. Res.,* **111,** D12106, doi:10.1029/2005JD006548.

Chen, X. L., H. M. Zhao, P. X. Li, and Z. Y. Yin, 2006: Remote sensing image-based analysis of the relationship between urban heat island and land use/cover changes. *Remote Sens. Environ.,* **104,** 133–146.

Cotton, W. R., and R. A. Pielke Sr., 2007: *Human Impacts on Weather and Climate*. 2nd ed. Cambridge University Press, 330 pp.

Davey, C. A., and R. A. Pielke Sr., 2005: Microclimate exposures of surface-based weather stations—Implications for the assessment of long-term temperature trends. *Bull. Amer. Meteor. Soc.,* **86,** 497–504.

De Noblet-Ducoudre, N., and A. Pitman, 2007: LUCID Land-Use and Climate, Identification of robust impacts. *iLEAPS Newsletter,* No. 4, iLEAPS International Project Office, Helsinki, Finland, 46–47.

Elvidge, C. D., K. E. Baugh, J. B. Dietz, T. Bland, P. C. Sutton, and H. W. Kroehl, 1999: Radiance calibration of DMSP-OLS low-light imaging data of human settlements. *Remote Sens. Environ.,* **68,** 77–88.

Fall, S., D. Niyogi, R. A. Pielke Sr., A. Gluhovsky, E. Kalnay, and G. Rochon, 2010a: Impacts of land use land cover on temperature trends over the continental United States: Assessment using the North American Regional Reanalysis. *Int. J. Climatol.,* **30,** 1980–1993, doi:10.1002/joc.1996.

Feddema, J. J., K. W. Oleson, G. B. Bonan, L. O. Mearns, L. E. Buja, G. A. Meehl, and W. M. Washington, 2005: The importance of land-cover change in simulation future climates. *Science,* **310,** 1674–1678.

Foley, J. A., and Coauthors, 2005: Global consequences of land use. *Science,* **309,** 570–574, doi:10.1126/science.1111772.

Hale, R. C., K. P. Gallo, T. W. Owen, and T. R. Loveland, 2006: Land use/land cover change effects on temperature trends at U.S. Climate Normals stations. *Geophys. Res. Lett.,* **33,** L11703, doi:10.1029/2006GL026358.

——, ——, and T. R. Loveland, 2008: Influences of specific land use/land cover conversions on climatological normals of near-surface temperature. *J. Geophys. Res.,* **113,** D14113, doi:10.1029/2007JD009548.

Hansen, J., R. Rudey, J. Glascoe, and M. Sato, 1999: GISS analysis of surface temperature change. *J. Geophys. Res.,* **104,** 30 997–31 022, doi:10.1029/1999JD900835.

——, R. Ruedy, M. Sato, M. Imhoff, W. Lawrence, D. Easterling, T. Peterson, and T. Karl, 2001: A closer look at the United Sates and global surface temperature change. *J. Geophys. Res.,* **106,** 23 947–23 963.

Imhoff, M. L., W. T. Lawrence, D. C. Stutzer, and C. D. Elvidge, 1997: A technique for using composite DM SP/OLS ''City Lights'' satellite data to map urban area. *Remote Sens. Environ.,* **61,** 361–370.

——, J. T. Compton, W. T. Lawrence, and D. C. Stutzer, 2000: The use of multisource satellite and geospatial data to study the effect of urbanization on primary productivity in the United States. *IEEE Trans. Geosci. Remote Sens.,* **38,** 2549–2556.

Jones, P. D., 1994: Hemispheric surface air temperature variations: A reanalysis and an update to 1993. *J. Climate,* **7,** 1794–1802.

——, and A. Moberg, 2003: Hemispheric and large-scale surface air temperature variations: An extensive revision and an update to 2001. *J. Climate,* **16,** 206–223.

Kabat, P., and Coauthors, 2004: *Vegetation, Water, Humans and the Climate: A New Perspective on an Interactive System*. Springer, 566 pp.

Kalnay, E., and M. Cai, 2003: Impact of urbanization and land-use change on climate. *Nature,* **423,** 528–531.

Klein Goldewijk, K., 2001: Estimating global land use change over the past 300 years: The HYDE database. *Global Biogeochem. Cycles,* **5,** 417–434.

——, and G. van Drecht, 2006: HYDE 3: Current and historical population and land cover. *Integrated Modelling of Global Environmental Change. An Overview of IMAGE 2.4.,* A. F. Bouwman, T. Kram, and K. Klein Goldewijk, Eds., Netherlands Environmental Assessment Agency (MNP), 93–111.

Lim, Y.-K., M. Cai, E. Kalnay, and L. M. Zhou, 2005: Observational evidence of sensitivity of surface climate changes to land types and urbanization. *Geophys. Res. Lett.,* **32,** L22712, doi:10.1029/2005GL024267.

Mahmood, R., and Coauthors, 2010: Impacts of land use/land cover change on climate and future research priorities. *Bull. Amer. Meteor. Soc.,* **91,** 37–46.

Menne, M. J., C. N. Williams Jr., and M. A. Palecki, 2010: On the reliability of the U.S. surface temperature record. *J. Geophys. Res.,* **115,** D11108, doi:10.1029/2009JD013094.

National Research Council, 2005: *Radiative Forcing of Climate Change: Expanding the Concept and Addressing Uncertainties*. National Academies Press, 224 pp.

Oke, T. R., 1987: *Boundary Layer Climates*. 2nd ed. John Wiley & Sons, 464 pp.

——, and J. E. Hay, 1998: *The Climate of Vancouver*. 2nd ed. BC Geographical Series, No. 50, University of British Columbia, 48 pp.

Olson, J. S., 1994a: Global ecosystem framework–Definitions. USGS EROS Data Center Internal Rep., 37 pp.

——, 1994b: Global ecosystem framework—Translation strategy. USGS EROS Data Center Internal Rep., 39 pp.

Peterson, T. C., 2006: Examination of potential biases in air temperature caused by poor station locations. *Bull. Amer. Meteor. Soc.,* **87,** 1073–1080.

——, and R. S. Vose, 1997: An overview of the Global Historical Climatology Network temperature database. *Bull. Amer. Meteor. Soc.,* **78,** 2837–2849.

——, T. R. Karl, P. F. Jamason, R. Knight, and D. R. Easterling, 1998: First difference method: Maximizing station density for the calculation of long-term global temperature change. *J. Geophys. Res.,* **103** (D20), 25 967–25 974.

Pielke, R. A., Sr., 2005: Land use and climate change. *Science,* **310,** 1625–1626.

——, and R. Avissar, 1990: Influence of landscape structure on local and regional climate. *Landscape Ecol.,* **4,** 133–155.

——, and D. Niyogi, 2010: The role of landscape processes within the climate system. *Landform—Structure, Evolution, Process Control: Proc. of the Int. Symp. on Landforms Organised by the Research Training Group 437,* J. C. Otto and R. Dikaum, Eds., Lecture Notes in Earth Sciences Vol. 115, Springer, 67–85, doi:10.1007/978-3-540-75761-0_5.

——, T. Stohlgren, W. Parton, N. Doesken, J. Moeny, L. Schell, and K. Redmond, 2000: Spatial representativeness of temperature measurements from a single site. *Bull. Amer. Meteor. Soc.,* **81,** 826–830.

——, and Coauthors, 2002: Problems in evaluating regional and local trends in temperature: An example from eastern Colorado, USA. *Int. J. Climatol.,* **22,** 421–434.

——, and Coauthors, 2007a: Documentation of uncertainties and biases associated with surface temperature measurement sites for climate change assessment. *Bull. Amer. Meteor. Soc.,* **88,** 913–928.

——, and Coauthors, 2007b: Unresolved issues with the assessment of multi-decadal global land surface temperature trends. *J. Geophys. Res.,* **112,** D24S08, doi:10.1029/2006JD008229.

Pitman, A. J., and Coauthors, 2009: Uncertainties in climate responses to past land cover change: First results from the LUCID intercomparison study. *Geophys. Res. Lett.,* L14814, doi:10.1029/2009GL039076.

Roy, S. S., R. Mahmood, D. Niyogi, M. Lei, S. A. Foster, K. G. Hubbard, E. Douglas, and R. A. Pielke Sr., 2007: Impacts of the agricultural Green Revolution–induced land use changes on air temperatures in India. *J. Geophys. Res.,* **112,** D21108, doi:10.1029/2007JD008834.

Shukla, J., C. Nobre, and P. Sellers, 1990: Amazon deforestation and climate change. *Science,* **247,** 1322–1325.

Small, C., F. Pozzi, and C. D. Elvidge, 2005: Spatial analysis of global urban extent from DMSP-OLS night lights. *Remote Sens. Environ.,* **96,** 277–291.

Smith, T. M., and R. W. Reynolds, 2005: A global merged land and sea surface temperature reconstruction based on historical observations (1880–1997). *J. Climate,* **18,** 2021–2036.

Solomon, S., D. Qin, M. Manning, M. Marquis, K. Averyt, M. M. B. Tignor, H. L. Miller Jr., and Z. Chen, Eds., 2007: *Climate Change 2007: The Physical Science Basis*. Cambridge University Press, 996 pp.

Turner, B. L., E. F. Lambin, and A. Reenberg, 2007: The emergence of land change science for a global environmental change and sustainability. *Proc. Natl. Acad. Sci. USA,* **104,** 20 666–20 671, doi:10.1073/pnas.0704119104.

Wichansky, P. S., L. T. Steyaert, R. L. Walko, and C. P. Weaver, 2008: Evaluating the effects of historical land cover change on summertime weather and climate in New Jersey: Land cover and surface energy budget changes. *J. Geophys. Res.,* **113,** D10107, doi:10.1029/2007JD008514.